ELSEVIER

NIM B

Beam Interactions
with Materials & Atoms

The AUSTRALIS microbeam ion source

S.H. Sie *, T.R. Niklaus, G.F. Suter

Heavy Ion Analytical Facility, CSIRO Exploration and Mining, P.O. Box 136, North Ryde, NSW 2113, Australia

Abstract

The AUSTRALIS (AMS for Ultra Sensitive TRAce eLement and Isotopic Studies) system being developed at the HIAF laboratory is a microbeam AMS system designed for in situ microanalysis of geological samples. The microbeam source was implemented by modifying a HICONEX source, resulting in a versatile source for microbeam as well as high intensity macrobeam operations. The source features a high magnification sample viewing system, enabling live observation of the sputtering process and visual tuning of the primary beam. Microbeam of Cs^+ as small as 30 μm in diameter has been obtained in the tests. The secondary ion extraction system features a "screen" electrode that is used to correct the primary beam trajectory affected by the extraction field, in order to return it to the geometric center of the sample. The paper will describe the source, and results of the test of the source and the injector system.

1. Introduction

The AUSTRALIS (AMS for Ultra-Sensitive TRAce eLement and Isotopic Studies) being developed at the CSIRO HIAF laboratory in Sydney, Australia is designed to enable AMS analysis with spatial resolution in the μm regime [1–3]. All rocks are typically composed of a mixture of monomineralic grains, ranging from typically μm to cm (macrocrysts). An ideal source would be that is capable of analysis of microscopic sample to bulk analysis.

An important feature of the source is the ability to view the sample, to facilitate locating the particular grain with micrometer precision. A microbeam source fulfilling these requirements has been developed by exploiting a number of features of the General Ionex Model 834 HICONEX source. A mass analysis system for the primary beam will be added in the second stage, to eliminate contamination of the samples by impurities in the primary beam. This paper presents the description of the ion source in detail, and initial results of the tests.

2. The microbeam source

The AUSTRALIS injector system consists of the sample chamber with provisions for two ion sources, and a

beam analysis system consisting of a 45° spherical electrostatic analyser (ESA) and 90° analysing magnet, both with 30 cm radius and double focusing. The first microbeam Cs^+ ion source now completed is constructed by modifying an existing HICONEX 834 source. The microbeam strikes the sample mounted at the centre of the chamber on a three-axis microstage, at 45° incidence angle. These features can be seen in Fig. 1, showing also the vacuum lock for sample exchange on the left hand side, and the zoom microscope equipped with a CCD camera. Sample can be exchanged in less than 10 min including pump down time. The sample stage has a positioning resolution 0.5 μm. The target ladder can accommodate three discs with 25 mm diameter, or thin sections (microscope slides). Alignment of the targets can be checked through the glass window in the back port.

In the normal mode of operation of the HICONEX source, the Cs^+ beam sputters a suitable target material incorporated into the surface of a "cone", and the negative secondary ions are extracted through the aperture in the cone. A magazine accommodates 12 cones which can be selected externally. The Cs^+ beam is produced by a gun, held at ground potential, consisting of a reservoir of Cs and a frit ioniser.

The details of the modification to the source are shown in Fig. 2. The Cs^+ beam is now extracted through the cone aperture, by replacing the secondary extraction electrode with a "Faraday cage" biased at the Cs^+ beam extraction voltage, enclosing the beam trajectory up to the microbeam lens. The aperture now serves as the object of the primary microbeam lens system, comprised of a condenser lens,

* Corresponding author. Tel. +61 2 887 8648, fax +61 2 887 8921, e-mail: s.sie@dem.csiro.au.
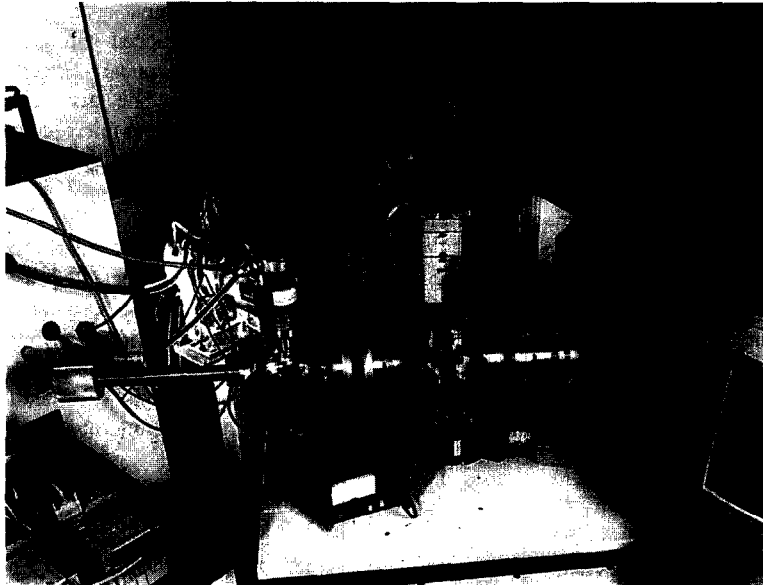
Fig. 1. A photograph of the sample chamber showing the sample microstage on the right hand side, the vacuum lock for sample exchange on the left hand side, and the zoom microscope equipped with a CCD camera. The sample stage has a positioning resolution 0.5 μm.
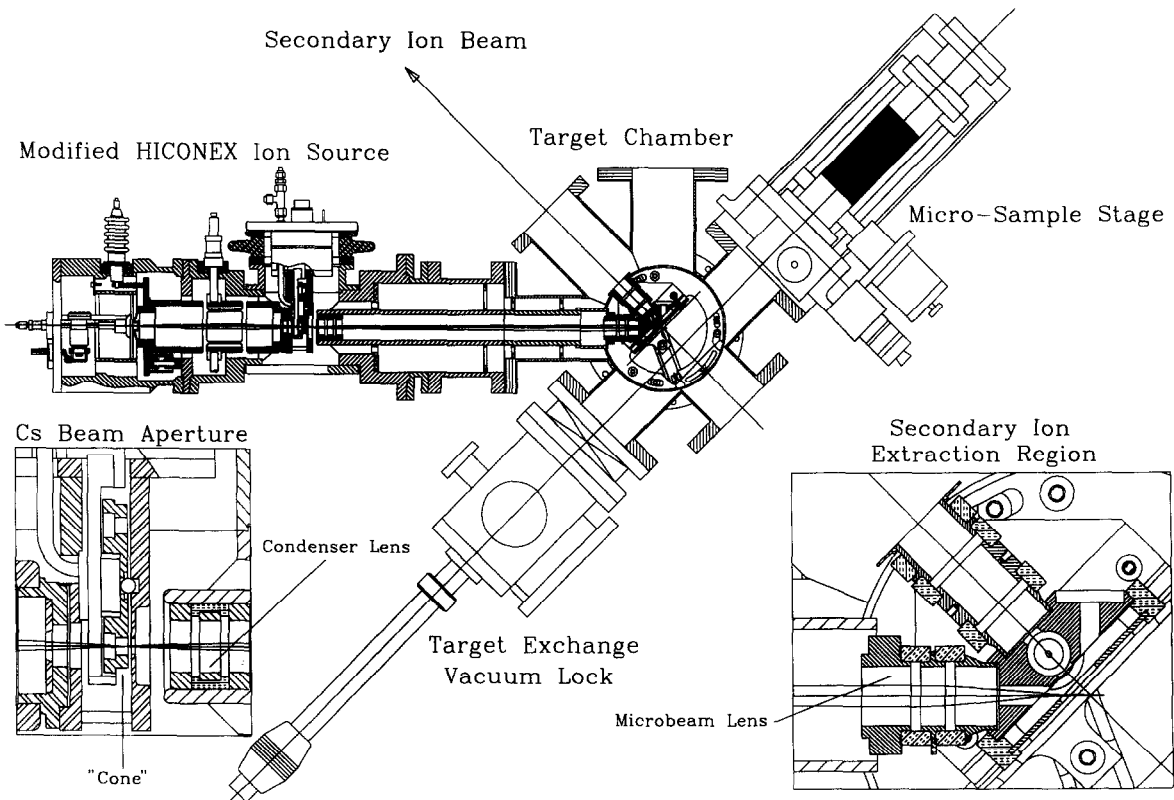

Fig. 2. A diagram showing the details of the modification to the HICONEX source, and the secondary ion extraction region. The Cs^+ beam is extracted through the cone aperture, which now serves as the object aperture of the primary microbeam lens system which consists of a condenser lens, the final focusing einzel lens near the target sample. The secondary ions are extracted and focused by an immersion lens sharing a common electrode (the extractor "block") with the primary system.

with the active element at ground potential and the final focusing einzel lens near the sample. The secondary ions are extracted and focused by an immersion lens sharing a common electrode (the extractor "block") with the primary system. A second einzel lens focuses the secondary ion beam at the object slits of the ESA. A "screen" electrode is interposed between the extractor block and the target to correct the trajectory of the primary beam affected by the secondary ion extraction field [1,2].

The samples are viewed by means of a zoom microscope combined with a stainless steel mirror, with a hole colinear with the secondary beam axis, housed in the extractor block. The optical magnification is further increased using a CCD camera, allowing positioning of samples with 1 μm pixel accuracy. By fixing the micro-

scope focus the sample distance from the extraction electrodes can be positioned within a few μm, ensuring that the ion optics of secondary extraction region is not altered when moving from one target spot to another. The total working distance of the microscope objective is 71 mm. In the present arrangement, the mirror is set at 27 mm from the target, defining the working distance of the primary microbeam lens system.

Fig. 3 shows the microbeam optics of the modified HICONEX source, calculated using the code SIMION vers. 5 [4] in cylindrical symmetry geometry. The source einzel is focused such that the exit beam from the condenser lens is approximately parallel, and the best focus at the target was obtained at around −400 V bias for the active element of the microbeam einzel. After this lens, the
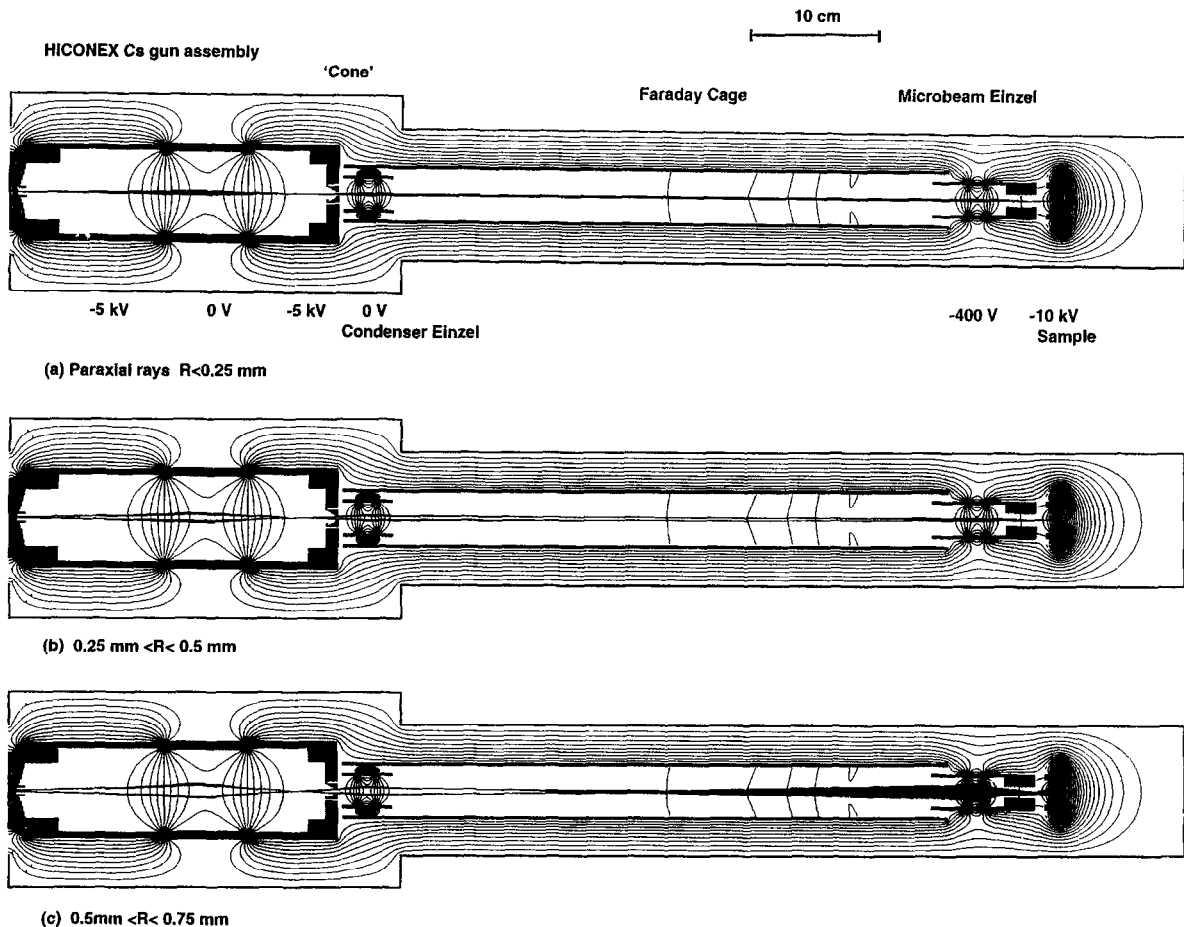

Fig. 3. The beam optics of the modified HICONEX source calculated using the code SIMION vers. 5 [4] in a cylindrically symmetric geometry. The equipotentials are spaced 500 V apart. a) Ray trace for paraxial rays confined to the source area (frit) of less than 0.25 mm radius. The resultant image is 20 μm in diameter. b) Ray trace for non-paraxial rays originating from an annulus at the frit between 0.25 and 0.5 mm radius. The image size increases to 300 μm. c) Ray trace from non-paraxial rays between 0.5 and 0.75 mm radius of the frit, showing a highly aberrated image. The contribution of non-paraxial rays can be controlled by selecting appropriate cone aperture diameters.

Cs is accelerated to the target which is biased at the secondary ion extraction voltage of -10 kV. The equipotentials are spaced 500 V apart. Fig. 3a shows the ray trace for paraxial rays confined to the source area (frit) of less than 0.25 mm radius. The resultant image is 20 μm in diameter. Fig. 3b shows the ray trace for non-paraxial rays originating from an annulus at the frit between 0.25 and 0.5 mm radius. The image size increases to 300 μm. Fig. 3c shows the ray trace from non-paraxial rays between 0.5 and 0.75 mm radius of the frit, with a highly aberrated image. From the figure it is obvious that the contribution of non-paraxial rays can be controlled by selecting appropriate cone aperture diameters. A 2 mm diameter aperture passes through all rays shown. In microbeam production, the size of usable part of the frit defines the maximum intensity that can be obtained.

The calculation represents the most optimistic result, in the absence of known emittance of the ionizing surface and space charge effects. Heated tungsten surface can produce as much as ~ 2 mA/cm^2 Cs$^+$ beam at $\sim 1500°$ [5]. Using this figure the maximum intensity at 20 μm resolution is thus ~ 4 μA, assuming all rays are focused as shown, corresponding to 1270 mA/cm2. This is much higher than the beam density of ~ 140 mA/cm^2 obtained in a typical HICONEX source, reflecting poorer phase space distribution due to other effects, e.g. poor surface texture of the ionizer that will increase beam divergence, as well as aberration effects.

Fig. 4 shows the optics of the secondary ion extraction region, featuring the "screen" electrode, calculated using the program SIMION. Because of cylindrical symmetry restrictions, the primary beam is simulated by a bundle of rays converging at the geometric center. For clearer definition of the centre, two symmetric bundles of primary rays are shown. The "screen" electrode serves two functions: first to screen the primary beam as much as possible from the secondary extraction field that will affect its trajectory, and second to correct the deviation caused by the field by tailoring the shape of the field to return the beam spot to the desired geometric center of the target. The latter is important in order to eliminate steering of the secondary ions to obtain the best mass and energy resolution for the injector, and also facilitates high magnification viewing of the sample, considering that for 1 μm pixel resolution the field of view is only 700 μm wide.

When the screen is set at the same potential as the "extractor block", the primary beam can be seen to deviate from the centre (Fig. 4). The effect would be even larger if the screen were removed. By varying the screen voltage slightly, the spot can be returned to the center. The displacement is approximately linear with the voltage difference between the screen and the extractor voltage. This electrode can therefore be used also to correct deviation caused by residual misalignment of the primary beam axis, provided that it is on the same plane as the secondary axis.

3. Source tests

With the facility to observe the target "live", the effect of the adjusting the screen electrode voltage can be seen in Fig. 5 showing a series of the video monitor screen frames. This allows visual tuning of the primary beam, and positioning of the beam spot at the secondary ion optics axis.
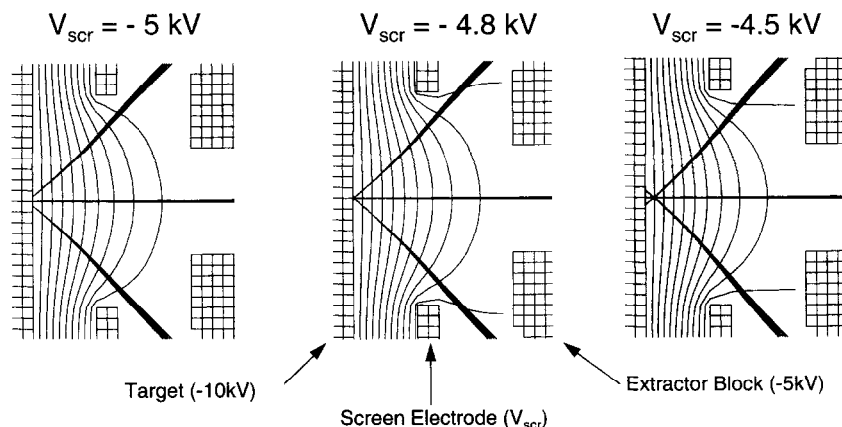

Fig. 4. The beam optics of the secondary ion system in cylindrical symmetry calculated with SIMION 5, showing the effect of the "screen" electrode. The primary ions are simulated using two symmetric bundles of rays converging at the centre of the target. The primary beam trajectory is affected by the extraction field, and the screen electrode voltage can be adjusted to correct it. The secondary ion optics is virtually unaffected by changes in the screen potential. The equipotential lines are 500 V apart.

Fig. 5. With the facility to observe the target at high magnification through a CCD camera, the effect of the adjusting the screen electrode voltage can be seen in the video monitor screen frames in this figure (row by row starting at the top left). The screen voltage is changed in one direction (frames 1 to 7) and returned almost to the initial value (last frame). The field of view is 1 mm wide.

The test results show good agreement with the calculated values of ~ 800 μm displacement for a 400 V change in the screen voltage, for a 5 keV Cs beam.

The beam can be observed readily using a carbon coated polished gold grain target (Fig. 6), as a bright erosion spot. The best focus for an uncollimated gun, i.e. when there is no cone in place corresponding to an aperture of 10 mm was 300 μm. The spot is an ellipse with $\sqrt{2}$ aspect ratio, consistent with a 45° incidence angle. Taking the short axis as the focus size, the best focus for a 2 mm aperture was 160 μm. A more uniform erosion spot but larger diameter (300 μm) is obtained when the beam intensity is not optimised at the target corresponding to the so-called "Koehler's illumination" mode [6]. Under this condition, the aperture is illuminated by the Cs beam focused to produce a waist before the aperture that coincides with the focal point of the condenser einzel, resulting in a parallel beam for the microbeam lens. Spherical aberration effects are minimized and the beam spot scales geometrically with the aperture size. The smallest aperture tried so far is 150 μm, resulting in a 30 μm spot size (Fig. 6).

4. Injector tests

The source and injector beam transport components are computer controlled through an Omron programmable logic controller system, run under LABVIEW software. The secondary ion einzel and the ESA are optimized by monitoring the beam in the Faraday cup at the ESA image point. This can be further optimized by monitoring the analyzed beam at the low energy magnet cup, with the exit slits wide open. In tests with $^{12}C^-$ beams, the ESA scans

show the difference in setting for an insulating sample (epoxy) of ~ 50 V against that for a conducting sample (graphite), demonstrating the effect of charge buildup in the insulating sample. The shape of the transmission peak reflects the kinetic energy distribution of the ions.

Molecular ions have a narrower energy distribution than atomic ions. The ESA voltage can be set at various portions of the transmission curve, and the exit slits at various widths to control the energy bandpass of the ESA. This energy filtering technique can be used to suppress the molecular ions. The effect can be demonstrated by mass scans of the injector magnet of a graphite target with the ESA set at the peak, and a few volts above the peak. In the latter the mass 13 peak intensity is lower, consistent with the lower molecular $^{12}CH^-$ ion portion at higher kinetic energy of the sputtered ions. Without defining slits, the mass 12 peak shows a broad flat top, consistent with the peak corresponding only to atomic ions of ^{12}C, while mass 13 shows a shape dependent on the setting of the ESA,

reflecting a varying mixture of molecular mass 13 ions.

Fig. 7 shows the mass scan of various targets with the magnet object slits set at 2 mm, corresponding to mass resolution of 300. At this setting, there is no loss in peak intensity for a 100 μm beam spot. The carbon peaks are present in all mass spectra due to the carbon coating on the samples. The oxygen peaks (mass 16 and 17) also occur in all spectra reflecting a relatively poor vacuum (10^{-6} Torr) in the sample chamber, or adsorbed oxygen on the surface.

The intensity of the primary beam can be estimated from the measured secondary ion intensity in the injector magnet Faraday cup. With the ioniser of the Cs gun at maximum setting and the Cs reservoir heated to 220°C, up to 1 nA of C was measured from the thin C coating at 30 μm resolution, and ~ 8 nA at 100 μm resolution (Fig. 7). For graphite targets a ~ 6% yield (12 keV Cs beam, 20 keV extraction) can be obtained [7]. Considering that in the present test the Cs energy and secondary extraction energy are lower, this efficiency may represent only the upper
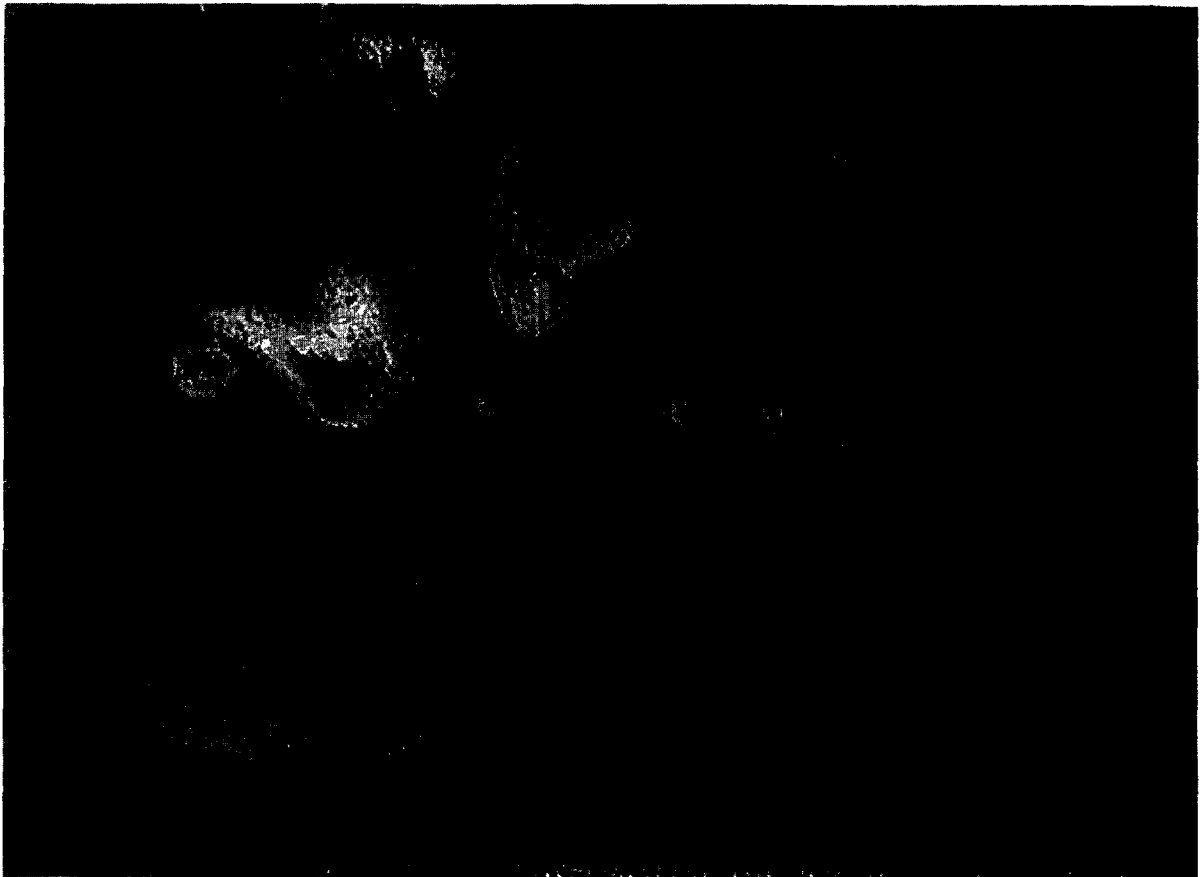

Fig. 6. The best focus of 30 μm obtained so far can be seen in this figure, showing a polished Au grain coated with a thin layer of carbon. The beam spot can be seen as bright spots that appear when the carbon is eroded by the beam. The field of view is 1.2 mm.
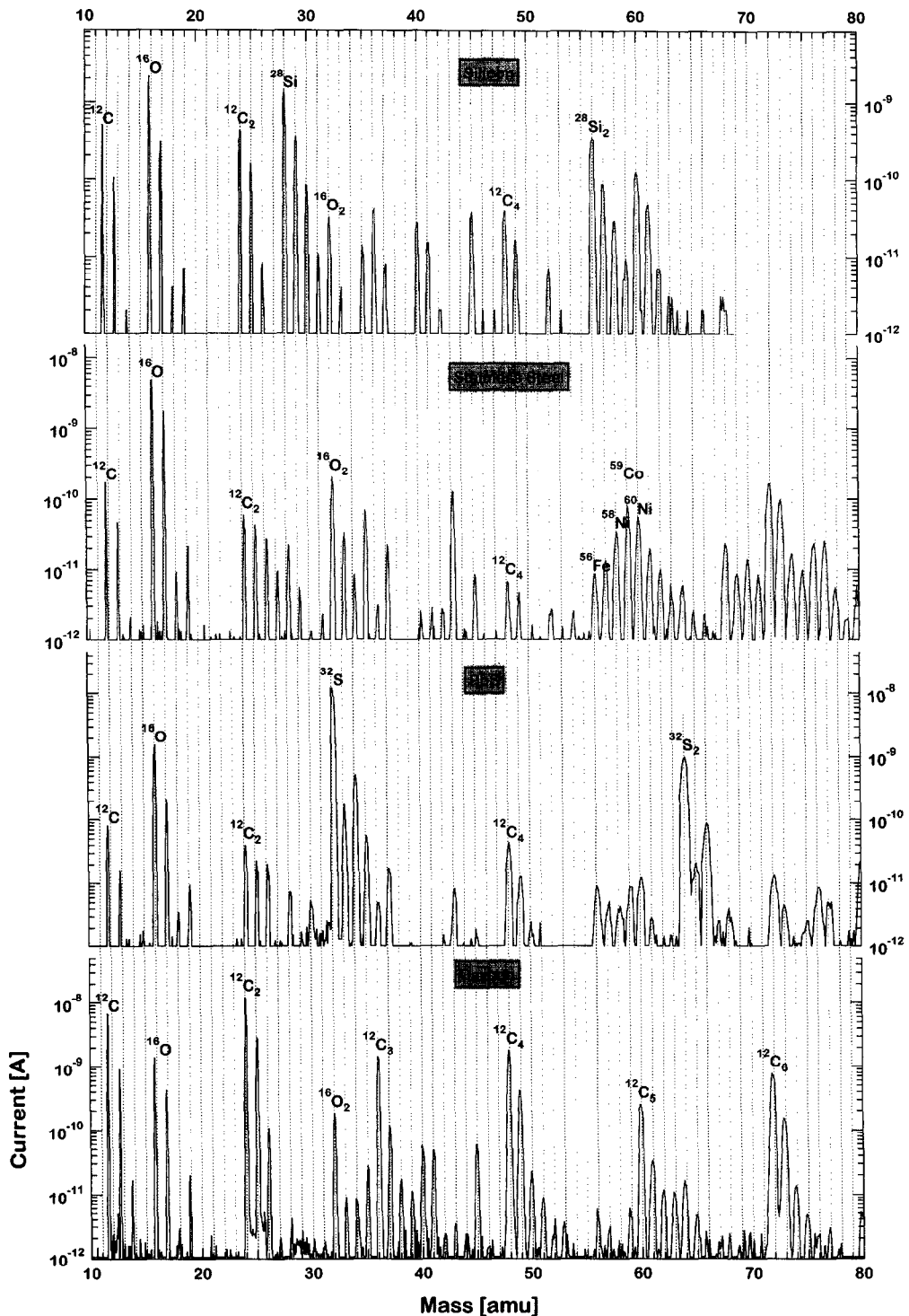
Fig. 7. Mass scans for Si, graphite, stainless steel and PbS targets, with the magnet object slits set at 2 mm, corresponding to mass resolution of 300. At this setting, there is no loss in peak intensity for a 100 μm beam spot.

limit. With this proviso we estimate that the intensity of the primary beam is at least 16 nA at 30 μm resolution, and 128 nA at 100 μm resolution corresponding to ∼ 2 and 1.6 mA/cm² beam density respectively. We believe that the low yield is mainly due to the problem with the frit. In the normal operation of the HICONEX source we

only managed to produce ~ 4 μA C⁻ beam, corresponding to ~ 64 μA Cs⁺ beam, well below the specification value of up to 100 μA. The present gun will be replaced in the near future. Misalignment of the beam transport components may explain the low source yield and the mass resolution being lower than the expected value. Better alignment procedure of the system is being investigated.

5. Conclusion

The AUSTRALIS microbeam source based on a modified HICONEX source proves to be a versatile device for providing Cs beam spanning the sub-milli and micron range of spatial resolution at maximum possible delivered intensity. The "screen" electrode in the secondary ion extraction region behaves as predicted and presents a convenient technique for correcting the effect of the secondary ion extraction field on the primary beam, giving a high degree of decoupling of the primary and secondary ion optics, as well as for correcting residual geometric misalignment of the lens axes. The facility for directly observing the sample with high magnification enables visual tuning of the primary beam for best resolution. The best microbeam resolution obtained so far is 30 μm. Estimate of the primary beam intensity indicates that we have not achieved the expected yield, which can be attributed to poor Cs⁺ gun performance. Tests of the injector system showed the sensitivity of the transmission and calibration on the conductivity of the target. The computer control of the beam transport elements facilitates the opti-

misation of the injector system. The injector system mass resolution achieved thus far is ~ 300, and with further test and better alignment of the beam transport elements the design specification is expected to be reached.

Acknowledgements

References

[1] S.H. Sie and G.F. Suter, Nucl. Instr. and Meth. 92 (1994) 221.
[2] S.H. Sie, T.R. Niklaus and G.F. Suter, Proc. of Heavy Ion Accelerator Technology Conf., Canberra, 1995, Nucl. Instr. and Meth. A 382 (1996) 299.
[3] S.H. Sie, T.R. Niklaus and G.F. Suter, these Proceedings. (AMS-7), Nucl. Instr. and Meth. B 123 (1997) 112.
[4] D.A. Dahl and J.E. Delmore, SIMION for PC/PS2 vers. 4.0, EGG-CS-7233 Rev. 2, April 1988 and version 5.0 for extended DOS (1994).
[5] A. Septier, in: Focusing of Charged Particles, ed. A. Septier, vol. 2 (Academic Press, New York, 1967) p. 123.
[6] H. Liebl, Vacuum 33 (1983) 525.
[7] R. Middleton, A Negative Ion Cookbook, University of Pennsylvania (1989) unpublished.